first-order transition does not exhibit any broadening as a function of pressure[16].

We conclude that the $T^{3/2}$ power law of the resistivity in MnSi and in related pure systems (under investigation) is not consistent with current models of itinerant-electron ferromagnetism. The origin of this form of $\rho(T)$ may lie in extremely subtle effects of disorder in the highest-purity samples, pointing at an entirely unexpected and new aspect of the metallic state. It is more likely, however, to lie in a diffusive motion of the electrons resulting from the interactions among the itinerant electrons themselves. This constitutes a breakdown of the Fermi-liquid or NFFL model, long assumed to be valid for the normal state of itinerant-electron ferromagnets. □

Received 2 August; accepted 12 September 2001.

1. Stoner, E. C. Collective electron ferromagnetism. *Proc. R. Soc. Lond. A* **165,** 372–414 (1938).
2. Radu, G. T. & Suhl, H. (eds) *Magnetism—A Treatise on Modern Theory and Materials* (Academic, New York, 1966).
3. Lonzarich, G. G. in *Electrons at the Fermi Surface* (ed. Springford, M.) 225–528 (Cambridge Univ. Press, Cambridge, 1980).
4. *Institute of Physics Conference on Non-Fermi Liquid Behaviour in Metals. J. Phys. Cond Matter.* (Spec. Issue) **8,** 9675–10148 (1996).
5. Varma, C. M., Nussinov, Z. & van Saarloos, W. Singular Fermi liquids. *Phys. Rep.* (in the press); also preprint cond-mat 0103393 at ⟨http://xxx.lanl.gov⟩.
6. Williams, H. J., Wernick, J. H., Sherwood, R. C. & Wertheim, G. K. Magnetic properties of monosilicides of some 3-d transition elements. *J. Appl. Phys.* **37,** 1256 (1966).
7. Plumer, M. L. & Walker, M. B. Wavevector and spin reorientation in MnSi. *J. Phys. C: Solid State Phys.* **14,** 4689–4699 (1981).
8. Ishikawa, Y. & Arai, M. Magnetic phase diagram of MnSi near critical temperature studied by neutron small angle scattering. *J. Phys. Soc. Jpn* **53,** 2726–2733 (1984).
9. Ishida, M. *et al.* Crystal chirality and helicity of the helical spin density wave in MnSi: II. polarized neutron diffraction. *J. Phys. Soc. Jpn* **54,** 2975–2982 (1985).
10. Lebech, B. in *Recent Advances in Magnetism of Transition Metal Compounds* 167–178 (World Scientific, Singapore, 1993).
11. Lonzarich, G. G. in *Electron* (ed. Springford, M.) 109–147 (Cambridge Univ. Press, Cambridge, 1997).
12. Pfleiderer, C. *et al.* Coexistence of superconductivity and ferromagnetism in the d-band metal $ZrZn_2$. *Nature* **412,** 58–61 (2001); Erratum *Nature* **412,** 660 (2001).
13. Fawcett, E., Maita, J. P. & Wernick, J. H. Magnetoelastic and thermal properties of MnSi. *Int. J. Magn.* **1,** 29–34 (1970).
14. Bloch, D., Voiron, J., Jaccarino, V. & Wernick, J. H. The high field–high pressure magnetic properties of MnSi. *Phys. Lett. A* **51,** 259–291 (1975).
15. Thompson, J. D., Fisk, Z. & Lonzarich, G. G. Perspective on heavy-electron and Kondo-lattice systems from high pressure studies. *Physica B* **161,** 317–323 (1989).
16. Pfleiderer, C., McMullan, G. J., Julian, S. R. & Lonzarich, G. G. Magnetic quantum phase transition in MnSi under hydrostatic pressure. *Phys. Rev. B* **55,** 8330–8338 (1997).
17. Thessieu, C. *et al.* Field dependence of the magnetic quantum phase transition in MnSi. *J. Phys. Condens. Matter* **9,** 6677–6687 (1997).
18. Ishikawa, Y. *et al.* Paramagnetic spin fluctuations in the weak itinerant-electron ferromagnet MnSi. *Phys. Rev. B* **31,** 5884–5893 (1985).
19. Yasuoka, H., Jaccarino, V., Sherwood, R. C. & Wernick, J. H. NMR and susceptibility studies of MnSi above T_c. *J. Phys. Soc. Jpn* **44,** 842–849 (1978).
20. Taillefer, L., Lonzarich, G. G. & Strange, P. The band magnetism of MnSi. *J. Magn. Magn. Mater.* **54–57,** 957–958 (1986).
21. Millis, A. J. Effect of a nonzero temperature on quantum critical points in itinerant fermion systems. *Phys. Rev. B* **48,** 7183–7196 (1993).
22. Goto, T., Shindo, Y., Takahashi, H. & Ogawa, S. Magnetic properties of the itinerant metamagnetic system $Co(S_{1-x}Se_x)_2$ under high magnetic field and high pressure. *Phys. Rev. B* **56**(21), 14019–14028 (1997).
23. Huxley, A., Sheikin, I. & Braithwaite, D. Metamagnetic behavior near the quantum critical point in UGe_2. *Physica B* **284–288,** 1277–1278 (2000).
24. Moriya, T. *Spin Fluctuations in Itinerant Electron Magnetism* (Springer, Berlin, 1985).
25. Lonzarich, G. G. & Taillefer, L. Effect of spin fluctuations on the magnetic equation of state of ferromagnetic or nearly ferromagnetic metals. *J. Phys. C* **18,** 4339–4371 (1985).
26. Varma, C. M. *et al.* Phenomenology of the normal state of Cu–O high-temperature superconductors. *Phys. Rev. Lett.* **63,** 1996–1999 (1989).
27. Ford, P. & Mydosh, J. A. Electrical resistivity of noble-metal-host-3d solute spin glass alloys. *Phys. Rev. B* **14,** 2057–2070 (1976).
28. Rivier, N. & Mensah, A. E. Low temperature resistivity and collective excitations. *Physica B* **91,** 85–88 (1977).
29. Fischer, K. H. On the electrical resistivity of spin glasses. *Z. Phys. B* **34,** 45–53 (1979).

Acknowledgements

We would like to thank N. R. Bernhoeft, S. Brown, P. Coleman, N. Doiron-Layraud, J. Flouquet, F. M. Grosche, S. M. Hayden, D. Khmelnitskii, H. v. Löhneysen, G. J. McMullen, A. J. Millis, A. Rosch, S. Sachdev, L. Taileffer, A. Tsvelik, T. Vojta and I. R. Walker. Financial support by the Deutsche Forschungsgemeinschaft (Germany), the Engineering and Physical Sciences Research Council (UK) and the European Science Foundation under FERLIN are gratefully acknowledged.

Correspondence and requests for materials should be addressed to C.P. (e-mail: christian.pfleiderer@physik.uni-karlsruhe.de).

Programmable and autonomous computing machine made of biomolecules

Yaakov Benenson*†, Tamar Paz-Elizur†, Rivka Adar†, Ehud Keinan‡§, Zvi Livneh† & Ehud Shapiro*†

** Department of Computer Science and Applied Mathematics, † Department of Biological Chemistry, Weizmann Institute of Science, Rehovot 76100, Israel*
‡ Department of Chemistry and Institute of Catalysis Science and Technology Technion – Israel Institute of Technology, Haifa 32000, Israel
§ Department of Molecular Biology and Skaggs Institute of Chemical Biology, The Scripps Research Institute, La Jolla, California 92037, USA

Devices that convert information from one form into another according to a definite procedure are known as automata. One such hypothetical device is the universal Turing machine[1], which stimulated work leading to the development of modern computers. The Turing machine and its special cases[2], including finite automata[3], operate by scanning a data tape, whose striking analogy to information-encoding biopolymers inspired several designs for molecular DNA computers[4–8]. Laboratory-scale computing using DNA and human-assisted protocols has been demonstrated[9–15], but the realization of computing devices operating autonomously on the molecular scale remains rare[16–20]. Here we describe a programmable finite automaton comprising DNA and DNA-manipulating enzymes that solves computational problems autonomously. The automaton's hardware consists of a restriction nuclease and ligase, the software and input are encoded by double-stranded DNA, and programming amounts to choosing appropriate software molecules. Upon mixing solutions containing these components, the automaton processes the input molecule via a cascade of restriction, hybridization and ligation cycles, producing a detectable output molecule that encodes the automaton's final state, and thus the computational result. In our implementation 10^{12} automata sharing the same software run independently and in parallel on inputs (which could, in principle, be distinct) in 120 μl solution at room temperature at a combined rate of 10^9 transitions per second with a transition fidelity greater than 99.8%, consuming less than 10^{-10} W.

A finite automaton[3] is a notional computing machine that operates on finite sequences of symbols. The machine can be in one of a finite number of internal states, of which one is designated an initial state and some are designated accepting states. Its software consists of transition rules, each specifying a next state based on the current state and the current symbol. It is initially positioned on the leftmost input symbol in the initial state. In each transition the machine moves one symbol to the right, changing its internal state according to one of the applicable transition rules. Alternatively, it may 'suspend' without completing the computation if no transition rule applies. A computation terminates on processing the last input symbol. An automaton is said to accept an input if a computation on this input terminates in an accepting final state.

The basic features and processes of a finite automaton with two internal states (S0 and S1) and an alphabet comprising two input symbols a and b are shown in Fig. 1. This automaton can have eight possible transition rules (T1–T8; Fig. 1c), and programming amounts to selecting some of these transition rules and deciding which internal states are accepting. There are 255 possible transition-rule selections and 3 possible selections of accepting states (either S0 or S1, or both), resulting in 765 syntactically distinct programs. A selection of such programs (A2–A7) is shown in Fig. 1d.

The design of our molecular finite automaton incorporates ideas

from designs for molecular Turing machines[5,8]. Its hardware consists of a mixture of the class IIS restriction nuclease *Fok*I, T4 DNA ligase and ATP, while the software comprises eight short double-stranded (ds) DNA molecules, the 'transition molecules' (Fig. 2a), which encode the eight possible transition rules (Fig. 1c). A dsDNA molecule encodes the initial state of the automaton and the input (Fig. 2b), with six base pairs (bp) coding for one input symbol (Fig. 2c). The system also contains 'peripherals', two output-detection molecules of different lengths (Fig. 2d), each of which can interact selectively with a different output molecule to form an output-reporting molecule that indicates a final state and can be readily detected by gel electrophoresis. The computation starts when the hardware, software and input are all mixed together and runs autonomously, if possible till termination. If the peripherals are also mixed then output reporters are formed *in situ* on termination.

The automaton processes the input as shown in Fig. 2e. First, the input is cleaved by *Fok*I, thereby exposing a four-nucleotide sticky end that encodes the initial state and the first input symbol. The computation proceeds via a cascade of transition cycles. In each cycle the sticky end of an applicable transition molecule ligates to the sticky end of the input molecule, detecting the current state and the current symbol. The product is cleaved by *Fok*I inside the next symbol encoding, exposing a new four-nucleotide sticky end. The design of the transition molecules ensures that the 6-bp-long encodings of the input symbols a and b are cleaved by *Fok*I at only two different 'frames'[5], the leftmost frame encoding the state S1 and the rightmost frame encoding S0 (Fig. 2c). The exact next restriction site and thus the next internal state are determined by the current state and the size of the spacers (Fig. 2a, green) in an applicable transition molecule. The computation proceeds until no transition molecule matches the exposed sticky end of the input or until the special terminator symbol is cleaved, forming an output molecule that has a sticky end encoding the final state. In a step extraneous to the computation and analogous to a 'print' instruction of a conventional computer, this sticky end ligates to one of two output detectors and the resultant output reporter is identified by gel electrophoresis.

We tested the operation of the automaton by running it with a selection of programs on various inputs (Fig. 3a). Each lane in the gel-electrophoresis image presents the result of running an indicated program on a specified input, showing the predicted output reporters in all cases or suspending where expected. The incorrect formation of a small amount of S1-R in an A6-aba computation and the formation of an unidentified product in an A5-aba computation are under investigation. Figure 3b shows computations of automaton A1 (Fig. 1a) on 6-symbol-long inputs, producing the expected outputs.

In all reactions, each input molecule initiates an independent parallel computation. Thus, the results depicted in Figs 3a and b represent 10^{12} automata operating in parallel. To illustrate this independence, we ran the same program on a mixture of two different inputs. Figure 3c shows that both output reporters were formed when expected. In the case of expected suspension on one of the inputs, a single correct reporter was formed.

We also tested a non-deterministic automaton A7 (Fig. 1d). Only computations on input aabb reached the accepting state S0, though some computations on this input reached state S1 and some suspended owing to different non-deterministic choices, as expected (Fig. 3d). Although the deterministic equivalent of A7 requires three states and cannot be programmed in our system, using a non-deterministic approach in real applications is disadvantageous as the yield decreases exponentially with the number of non-deterministic choices made during a computation.

We validated the mechanism of operation (Fig. 2e) by the results of three experiments: omission of single components, analysis of the intermediates, and measurement of computation fidelity (Fig. 4). First, we ran A1 on ababaa, omitting a single reaction component at a time (Fig. 4a). No output reporters could be detected once an essential component was omitted except for the case of T6 removal, an incorrectness similar to the case of the A6-aba computation. In addition, omitting ligase did not seem to impair the formation of the output molecule, although without ligase the reporter could not be detected. The possibility of ligase-free computing is under investigation.

In the second experiment, we analysed the sizes of computation

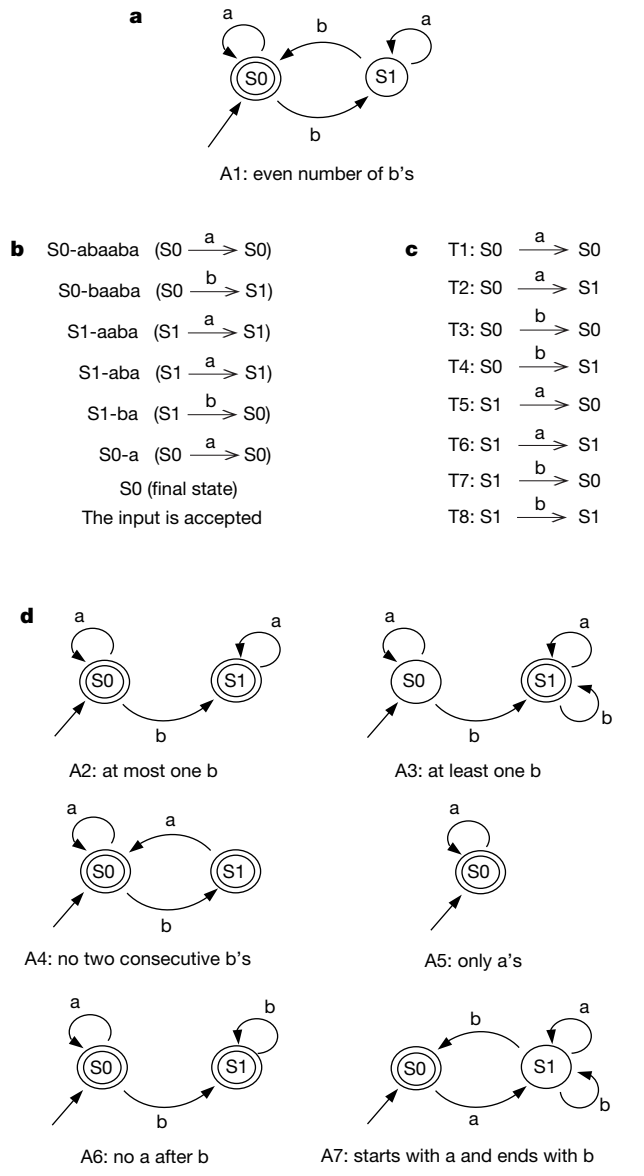

Figure 1 Finite automata with two states (S0 and S1) and two symbols (a and b). **a**, Diagram representing the automaton A1 accepting inputs with an even number of b symbols. Incoming unlabelled arrow represents the initial state, labelled arrows represent transition rules, and the double circle represents an accepting state. **b**, An example computation over abaaba. Each row represents an intermediate configuration, showing the current state of the automaton and the remaining symbols to be processed. The transition rule taking a configuration to its successor is shown on the right. **c**, A list of all eight possible transition rules of a two-state two-symbol automaton. **d**, Six other automata programs used to test the molecular implementation and the sets of inputs they accept. Non-deterministic automaton A7 has two transitions T7 and T8 applicable to the same configuration. A computation of A7 ending in an accepting state uses T8 for all b symbols except the last, and uses T7 for the last b.

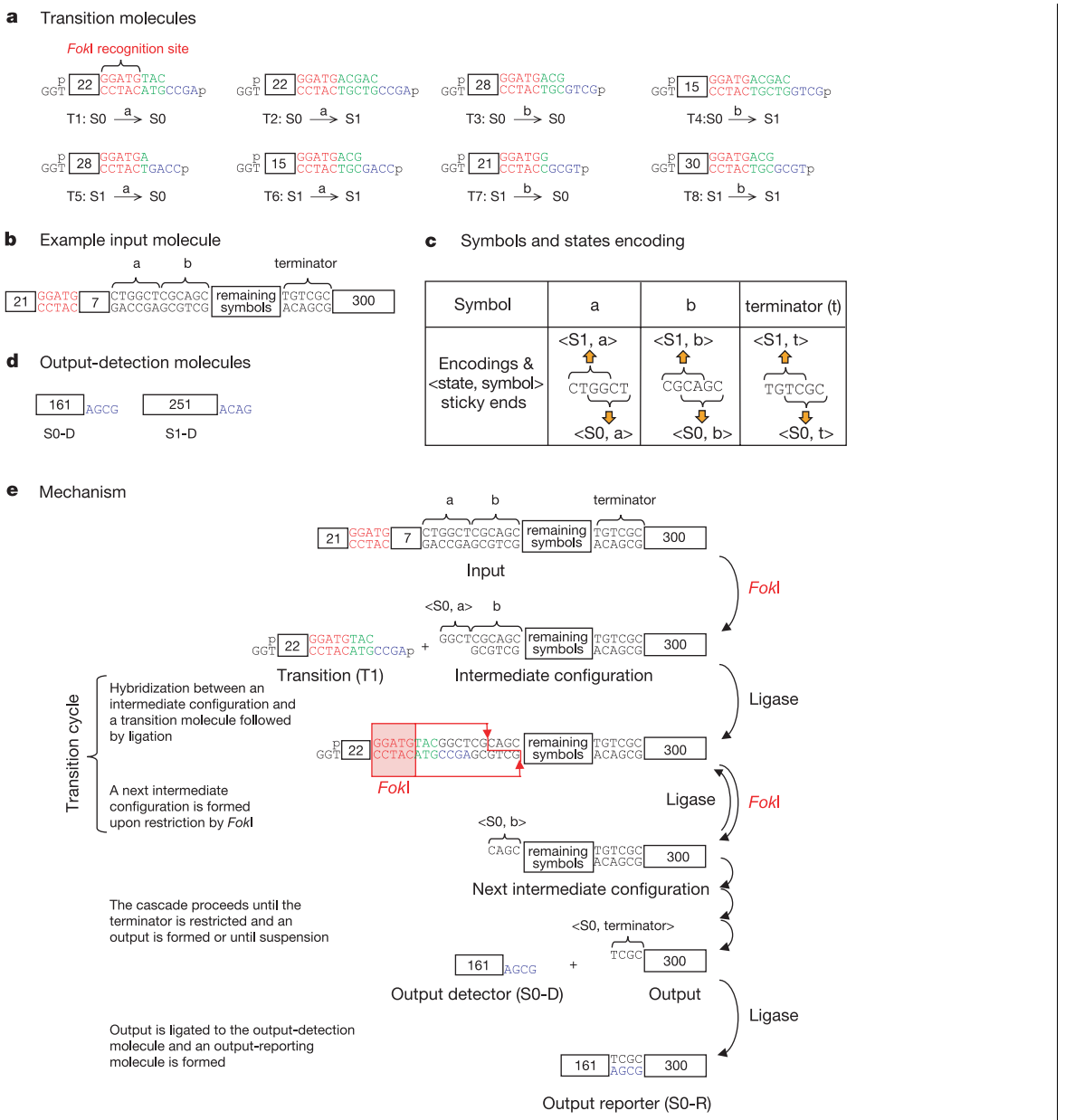

Figure 2 Design details and mechanism of operation of the molecular finite automaton. **a**, Structure of the transition molecules. A transition molecule detects the current state and symbol and determines the next state. It consists of ⟨state, symbol⟩ detector (blue), *Fok*I recognition site (red) and spacer (green) that determines the location of the *Fok*I cleavage site inside the next symbol encoding, which in turn defines a next state. 1-bp spacers effect S1 to S0 transition, 3-bp maintain the current state, and 5-bp transfer S0 to S1. **b**, Structure of an input molecule. **c**, The encoding for the input symbols a, b, and terminator (sense strands) and the sequences of the ⟨state, symbol⟩ sticky ends. **d**, Structure of the output-detection molecules. **e**, A sample processing of an input molecule beginning with ab. The S0 $\xrightarrow{a}$ S0 rule is applied to the first intermediate configuration molecule. The detection is illustrated for S0 output.

intermediates (Fig. 4b). The A1 program with input ababaa uses all its transition molecules in the order T1, T4, T6, T7 in the first four cycles. Thus, removal of each transition molecule would suspend the computation in each of its first four intermediates. These molecules would accumulate, 'waiting' for hybridization with the missing transition molecule, together with the product of the reverse ligation with a fragment restricted at the previous cycle (Fig. 2e). This experiment was performed with a ^{32}P-labelled ababaa input. The expected sizes of the intermediates were compared to the actual sizes obtained using a calibration curve based on the standards ladder. The correctness of this measurement is ±1% (±3.5 bp). The sizes of the 'restricted' (lower) bands are shown in the following (measured, predicted) pairs for each removed transition molecule: (-T1): (365 ± 4, 360); (-T4): (357 ± 4, 354); (-T6): (352 ± 4, 350); (-T7): (344 ± 4, 344). The differences between the lengths of the intermediates are 8, 5 and 8 bp between the first and second, second and third, and third and fourth intermediates, respectively. The predicted values are 6, 4 and 6 bp, respectively. These data support the proposed mechanism within the experimental error. More precise experiments are under way.

In the third experiment, we measured the computation fidelity by increasing the detection sensitivity using ^{32}P-labelled output detectors. In two computations with opposite predicted outputs, no incorrect products could be detected even after prolonged exposure. Given the detection limit, the overall fidelity of the computations is

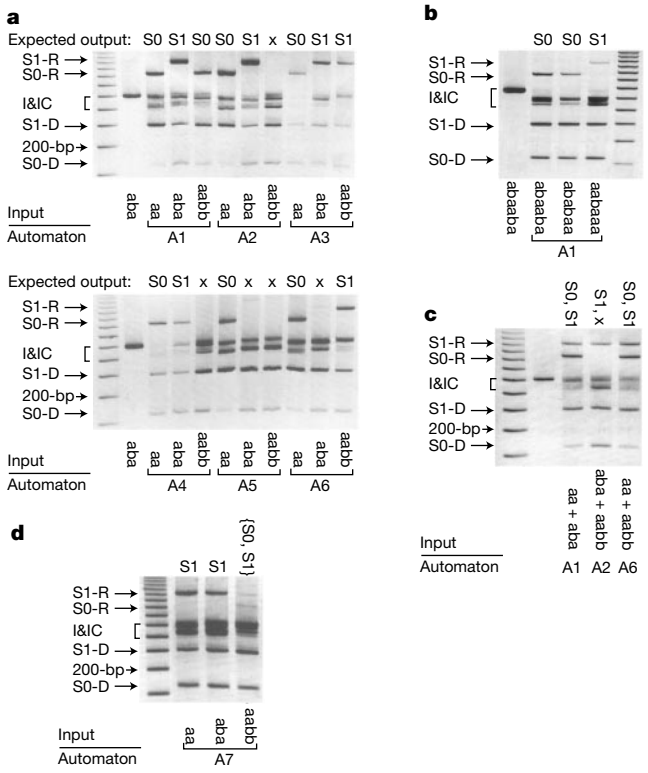

Figure 3 Running automaton programs on inputs. **a**, Experimental testing of automaton programs A1–A6 (Fig. 1a and d). The molecules in each lane are the output-detection molecules S0-D and S1-D, molecules encoding intermediate configurations capped by yet-to-be-processed input molecules and followed by output-reporting molecules S0-R or S1-R, which are missing in case the computation suspends (for example, A2, 'at most one b', suspends on aabb). Expected locations of different species and a size marker of 200 bp are indicated by arrows to the left. Input molecules are specified below each lane, and expected outputs (S0, S1 or suspension (x)) are indicated above each lane. Reactions with the same software are grouped in triplets, the software indicated below. I&IC, input and intermediate configurations. **b**, Computations with A1 software performed over 6-symbol-long input molecules. All inputs are of the same size, shown on a reference lane. **c**, Parallel computation. Input mixture composition and the software used are indicated below the lanes. **d**, Demonstration of a non-deterministic computation.

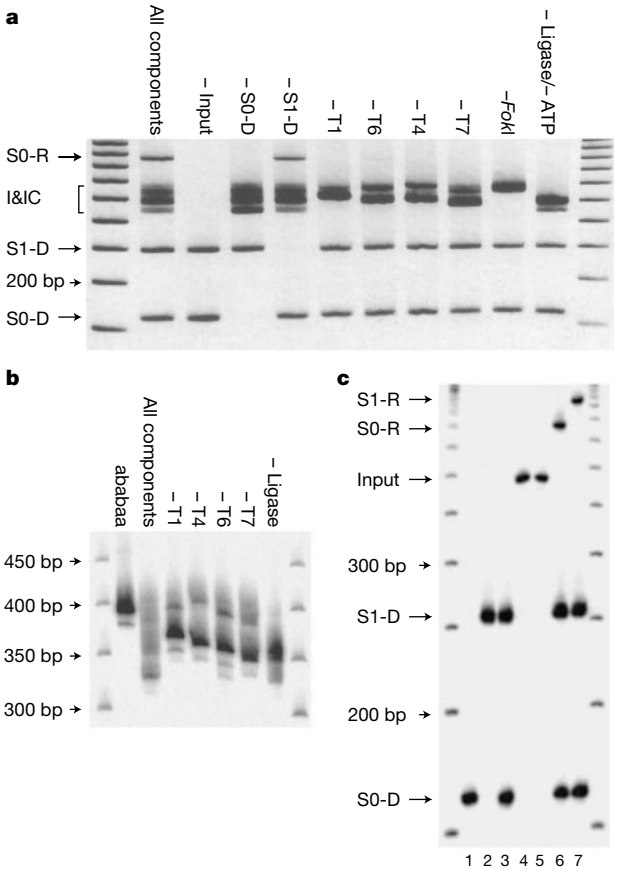

Figure 4 Verification of the operation mechanism. **a**, Identification of the essential components. Each lane is a computation reaction with one component omitted (above). The ligase or ATP-free reactions were identical and are represented by one lane. **b**, Close inspection of the reaction intermediates analysed by native PAGE (5%). Sample composition is indicated above the gel image. The ababaa lane contains labelled input. 'All components' lane is an output-detectors-free A1 computation, performed for reference. All other lanes lack the indicated components. The size markers are indicated to the left. **c**, An estimation of system fidelity analysed by native PAGE (6%). The composition of different lanes is as follows: 1, pure labelled S0-D; 2, pure labelled S1-D; 3, input-free computation reaction; 4, pure labelled ababaa; 5, pure labelled aabaaa; 6, a computation reaction over ababaa with unlabelled input and labelled output-detection molecules; 7, a similar reaction over aabaaa. Locations of the different components and the size markers of 200 bp and 300 bp are indicated on the left.

at least 99%, implying more than 99.8% fidelity per transition (Fig. 4c).

We have estimated the computing performance and energy consumption of the system. A computation over 2.5 pmol (1.5×10^{12} molecules) of a 4-symbol-long input rendered output-reporting molecules with ~50% yield, producing 7.5×10^{11} outputs in 4,000 s. As each output is the result of five transitions, the computing performance is of the order of 10^9 transitions per second. As for energy consumption—in each transition two ATP molecules were consumed, releasing 1.5×10^{-19} J. Multiplying this number by the transition rate provides an energy consumption rate of $\sim 10^{-10}$ J s^{-1}, or 10^{-10} W. Cost of construction of the input, software and hardware is not normally included when measuring the energy consumption of electronic computers and is not included here, although our present system will require recycling of 'software molecules' and of course additional energy to separate and 'read' the output via gel electrophoresis. This adds a significant continuing energy cost not normally encountered in electronic computers.

Any increase in the complexity of our system (number of symbols times the number of states) is bounded from above by the number of different non-palindromic sticky ends. The distribution between states and symbols depends on the length of the spacer between the recognition site and the restriction site of the particular restriction enzyme employed, with *Fok*I enabling a machine with at most three states and several tens of symbols. But the discovery or engineering of new class IIS enzymes with longer spacers and/or longer sticky ends[21] might allow the construction of automata with increased complexity, linearly related to size of the spacer and exponentially related to the size of the sticky end formed on restriction. □

Methods

Synthetic DNA

Double-stranded synthetic DNA molecules were prepared by annealing 2,000 pmol of commercially obtained deoxyoligonucleotides (Sigma-Genosys) in a final volume of 10 μl of 10 mM Tris-HCl buffer, pH 8.0, containing 1 mM EDTA and 50 mM NaCl. The annealing was performed by heating the solution to 94 °C followed by slow cooling. The formation of a duplex was confirmed by native PAGE (20%). The oligomers were 5′-phosphorylated and PAGE-purified by the supplier and used without further purification.

Input molecules

These were constructed stepwise by ligating one or more synthetic DNA segments of the

desired sequence to a 1,457-bp fragment obtained by digestion of the pBluescript II SK+ plasmid (Stratagene) with *Fok*I, followed by polymerase chain reaction (PCR) amplification of the coding segment and a 300- or 325-bp tail region. The sequences of the resulting input molecules were confirmed by sequencing.

Output-detecting molecules

The output-detecting molecule for the S0 output (S0-D) was formed by ligating a synthetic adapter of 30 bp containing a *Fok*I recognition site to a 181-bp fragment obtained by digesting the pBluescript II SK+ plasmid with *Fok*I, PCR amplification and additional *Fok*I digestion to form the 160-bp fragment bearing the desired sticky end. The output-detecting molecule for the S1 output (S1-D) was obtained by PCR amplification of a 285-bp fragment corresponding to positions 1,762–2,047 of the pBluescript II SK+ plasmid followed by *Fok*I digestion of the PCR product to form a 250-bp fragment.

Computation reactions

Reactions were set by mixing 2.5 pmol of the input molecule, 1.5 pmol of each output-detection molecule and 15 pmol of each transition molecule with 12 units of *Fok*I and 120 units of T4 DNA Ligase (both from New England Biolabs) in 120 μl of NEB4 buffer supplemented with 1 mM ATP and incubating at 18 °C for 70 min. In case of multiple inputs in the same reaction, equal amounts were used, summing up to 2.5 pmol. The mixtures were purified by the Qiagen PCR purification kit and eluted using 30 μl EB buffer (Qiagen). Aliquots (10 μl) were assayed by gel electrophoresis using 3% MetaPhor agarose (FMC Bioproducts) unless indicated otherwise. The lengths of the DNA species were verified using a commercial 50-bp DNA step ladder (Promega). To further confirm that output reporting molecules were formed as expected, we amplified by PCR and sequenced the output-detection molecule/output molecule junction region in both output-reporting molecules S0-R and S1-R and found the expected sequences (not shown).

Received 24 January; accepted 21 September 2001.

1. Turing, A. M. On computable numbers, with an application to the Entcheidungproblem. *Proc. Lond. Math. Soc. II Ser.* **42,** 230–265 (1936).
2. Hopcroft, J. E., Motwani, R. & Ullman, J. D. *Introduction to Automata Theory, Languages and Computation* 2nd edn (Addison-Wesley, Boston, Massachusetts, 2000).
3. McCulloch, W. S. & Pitts, W. A logical calculus immanent in nervous activity. *Bull. Math. Biophys.* **5,** 115–133 (1943).
4. Bennet, C. H. The thermodynamics of computation—a review. *Int. J. Theor. Phys.* **21,** 905–940 (1982).
5. Rothemund, P. W. K. in *DNA Based Computers: Proceedings of the DIMACS Workshop, April 4, 1995, Princeton University* (eds Lipton, R. J. & Baum, E. B.) 75–119 (American Mathematical Society, Providence, Rhode Island, 1996).
6. Smith, W. D. in *DNA Based Computers: Proceedings of the DIMACS Workshop, April 4, 1995, Princeton University* (eds Lipton, R. J. & Baum, E. B.) 121–185 (American Mathematical Society, Providence, Rhode Island, 1996).
7. Garzon, M. *et al.* in *Automata Implementation: Lecture Notes in Computer Science 1436* (eds Wood, D. & Yu, S.) 56–74 (Springer, Berlin, 1998).
8. Shapiro, E. & Karunaratne, K. S. G. Method and system of computing similar to a Turing machine. US Patent 6,266,569 (2001).
9. Adelman, L. M. Molecular computation of solutions to combinatorial problems. *Science* **266,** 1021–1024 (1994).
10. Lipton, R. J. DNA solution of hard computational problem. *Science* **268,** 542–545 (1995).
11. Ouyang, Q., Kaplan, P. D., Liu, S. & Libchaber, A. DNA solution of the maximal clique problem. *Science* **278,** 446–449 (1997).
12. Landweber, L. F., Lipton, R. J. & Rabin, M. O. in *DNA Based Computers III: DIMACS Workshop, June 23-27, 1997, University of Pennsylvania* (eds Rubin, H. & Wood, D. H.) 161–172 (American Mathematical Society, Providence, Rhode Island, 1997).
13. Liu, Q. *et al.* DNA computing on surfaces. *Nature* **403,** 175–179 (2000).
14. Faulhammer, D., Cukras, A. R., Lipton, R. J. & Landweber, L. F. Molecular computation: RNA solutions to chess problems. *Proc. Natl Acad. Sci. USA* **97,** 1385–1389 (2000).
15. Ruben, A. J. & Landweber, L. F. The past, present and future of molecular computing. *Nature Rev. Mol. Cell Biol.* **1,** 69–72 (2000).
16. Winfree, E., Liu, F. R., Wenzler, L. A. & Seeman, N. C. Design and self-assembly of two-dimensional DNA crystals. *Nature* **394,** 539–544 (1998).
17. Sakamoto, K. *et al.* State transitions by molecules. *Biosystems* **52,** 81–91 (1999).
18. Hartemink, A. J., Gifford, D. K. & Khodor, J. Automated constraint-based nucleotide sequence selection for DNA computation. *Biosystems* **52,** 227–235 (1999).
19. Khodor, J. & Gifford, D. K. Design and implementation of computational systems based on programmed mutagenesis. *Biosystems* **52,** 93–97 (1999).
20. Mao, C., LaBean, T. H., Reif, J. H. & Seeman, N. C. Logical computation using algorithmic self-assembly of DNA triple-crossover molecules. *Nature* **407,** 493–496 (2000).
21. Chandrasegaran, S. & Smith, J. Chimeric restriction enzymes: What is next? *Biol. Chem.* **380,** 841–848 (1999).

Acknowledgements

We thank I. Sagi and A. Yonath for use of their laboratory for our first set of experiments, and S. Shuping, A. Regev and N. Kessler for assistance and advice. E.K. is the incumbent of the Benno Gitter and Ilana Ben-Ami Chair of Biotechnology, Technion. Z.L. is the Incumbent of The Maxwell Ellis Professorial Chair in Biomedical Research. This work was supported by the Dolphi and Lola Ebner Center for Biomedical Research.

Correspondence and requests for materials should be addressed to E.S. (e-mail: Ehud.Shapiro@weizmann.ac.il).

Superconductivity in $CaCuO_2$ as a result of field-effect doping

J. H. Schön*, M. Dorget†‡, F. C. Beuran†§, X. Z. Zu‡, E. Arushanov‡‖, C. Deville Cavellin†‡ & M. Laguës‡

* *Bell Laboratories, Lucent Technologies, 600 Mountain Avenue, Murray Hill, New Jersey 07974-0636, USA*
† *GPMD-Université Paris, 12-61 avenue De Gaulle, 94010 Créteil Cedex, France*
‡ *Surfaces et Supraconducteurs CNRS UPR5-ESPCI, 10 rue Vauquelin, 75005 Paris, France*
§ *Wintici SA, 17 rue Jean Moulin, 94 300 Vincennes, France*
‖ *Institute of Applied Physics, Academy of Sciences of the Moldova Republic, Academiei str. 5, Kishinev 277028, Moldova*

Understanding the doping mechanisms in the simplest superconducting copper oxide—the infinite-layer compound $ACuO_2$ (where A is an alkaline earth metal)—is an excellent way of investigating the pairing mechanism in high-transition-temperature (high-T_c) superconductors more generally[1–4]. Gate-induced modulation of the carrier concentration[5–7] to obtain superconductivity is a powerful means of achieving such understanding: it minimizes the effects of potential scattering by impurities, and of structural modifications arising from chemical dopants. Here we report the transport properties of thin films of the infinite-layer compound $CaCuO_2$ using field-effect doping. At high hole- and electron-doping levels, superconductivity is induced in the nominally insulating material. Maximum values of T_c of 89 K and 34 K are observed respectively for hole- and electron-type doping of around 0.15 charge carriers per CuO_2. We can explore the whole doping diagram of the CuO_2 plane while changing only a single electric parameter, the gate voltage.

In 1988 Siegrist *et al.* were the first to synthesize an infinite-layer copper oxide (ILCO)[8]. Because of their structural simplicity (Fig. 1), ILCOs are ideally suited as model systems providing insights into mechanisms of high-T_c superconductivity in copper oxides[9]. But the undoped compound, prepared[8] under ambient pressure with the composition $Ca_{0.86}Sr_{0.14}CuO_2$, exhibits only antiferromagnetic and no superconducting properties[10]. Later, n-type doping was obtained with the bulk compound $Sr_{1-x}Ln_xCuO_2$ ($x \leq 0.1$–0.15) synthesized under a pressure of 3–6 GPa (refs 1, 11–14). In addition, electron-doped, pseudomorphically stabilized thin films were also grown using various techniques[15–17]. Superconducting transitions were observed in these doped compounds with a maximum T_c

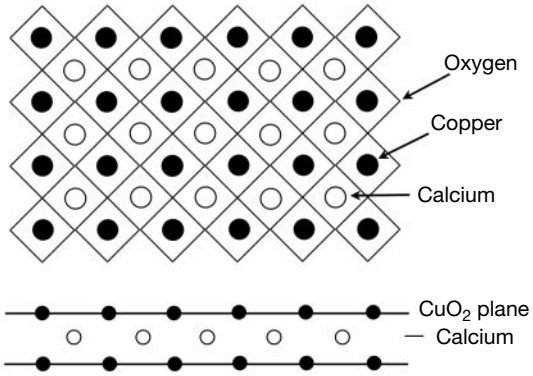

Figure 1 Schematic structure of the infinite-layer compound $CaCuO_2$. This is the 'parent structure' of the layered high-temperature superconductors. The structure is tetragonal, and consists of CuO_2 planes and cationic Ca planes, alternately stacked along the *c*-axis.